Underground imaging by frequency-domain electromagnetic migration

Michael S. Zhdanov*, Peter Traynin‡, and John R. Booker**

ABSTRACT

A new method of the resistivity imaging based on frequency-domain electromagnetic migration is developed. Electromagnetic (EM) migration involves downward diffusion of observed EM fields whose time flow has been reversed. Unlike downward analytical continuation, migration is a stable procedure that accurately restores the phase of the upgoing field inside the Earth. This method is indented for the processing and interpretation of EM data collected for both TE and TM modes of plane-wave excitation. Until recently, the method could be applied only for determining the position of anomalous structures and for finding interfaces between layers of different conductivity. There were no well developed approaches to the resistivity imaging, which is the key problem in the inversion of EM data. We provide a novel approach to determining not only the position of anomalous structures but their resistivity as well. The main difficulty in the practical realization of this approach is determining the background resistivity distribution for migration. We discuss the method of the solution of this problem based on differential transformation of apparent resistivity curves. The final goal of migration is to provide a first order interpretation using a computational effort equivalent to a forward modeling calculation.

INTRODUCTION

A problem of current practical interest is that of imaging inhomogeneous underground structures using surface or borehole electromagnetic data. The last decade has seen considerable improvement in the ability to gather spatially dense, accurate EM induction data. Improved extraction of structural information from such data is important for many practical applications ranging from mineral exploration to waste and building site characterization. Recently there has been considerable progress in the direct inversion of magnetotelluric and other low-frequency induction data for multidimensional electrical conductivity structures (Berdichevsky and Zhdanov, 1984; Smith and Booker, 19881991; Wannamaker et al., 1989; Eaton, 1989; Madden and Mackie, 1989; deGroot-Hedlin and Constable, 1990; Xiong and Kirsh, 1992; Lee and Xie, 1993; Oristaglio et al., 1993; Pellerin et al., 1993; Torres-Verdin and Habashy, 1994; Tripp and Hohmann, 1993; Oldenburg et al., 1993; 1994; Zhdanov and Keller, 1994). However, these algorithms require repeated solution of large multidimensional forward problems.

Several publications address simple and fast inversion techniques for transient electromagnetic data over inhomogeneous structures (Barnett, 1984; Macnae and Lamontagne, 1987; Eaton and Hohmann, 1989). The majority of these papers have been based on equating the transient response, measured at the surface of the Earth to the EM field of current filament images of the source. This approach originated in the pioneering work of Nabighian (1979) describing the behavior of transient currents diffusing into the earth as a system of "smoke rings" blown by the transmitting loop into the earth.

We will outline a different approach based on direct transformation of the observed wavefield into a resistivity image of the cross-section in a very rapid manner. We call this approach *electromagnetic migration*. The goal of migration is to provide a first-order interpretation using a computational effort equivalent to a forward model calculation.

The basic ideas of EM migration were first formulated in the papers by Zhdanov and Frenkel(1983a, b), where the integral approach to the solution of the problem of downward extrapolation in the reverse time has been exposed. The method described in those publications had two main limitations: first, the method is based on Stratton-Chu type integrals and therefore requires (in general) the observation of all six components of the EM field, which is difficult to realize in practice; second, it can be applied only to the models with the homogeneous background resistivity. The more advanced

analysis of this approach has been presented in part in the more recent publications: Zhdanov, 1988; Zhdanov et al., 1988 (in Russian); Zhdanov and Booker, 1993; and Zhdanov and Keller, 1994. However, during recent years the method has been significantly developed and improved. Now we have a much clearer understanding of the physical principles and mathematical foundations of EM migration. Until recently, the method could be applied only for determining the position of anomalous structures and for finding interfaces between layers of different conductivity. There were no well developed approaches to imaging the resistivity property itself, which is the key problem in the inversion of EM data.

We present a new method of the resistivity imaging based on frequency-domain electromagnetic migration. We develop this method for the processing and interpretation of EM data collected for both transverse electric (TE) and transverse magnetic (TM) modes of plane-wave excitation. To make the presentation clearer, we feel it necessary to begin our paper with a short review of the concepts of the migration as applied to interpretation of EM data. So, for completeness, in the first sections of this paper we will outline the physical principles and mathematical foundations of EM migration. We illustrate the method with numerical examples, typical for geoelectrical exploration.

PHYSICAL PRINCIPLES OF EM MIGRATION

The physical principles of EM migration parallel those underlying laser holography and seismic migration. The EM field produced by a controlled or natural source and observed on the earth's surface is the combination of two fields: a primary field that propagates downwards into the earth, and a secondary field that propagates upwards after having been scattered back from internal structure. Both fields satisfy diffusion equations inside the earth. Their amplitudes decay and their phases are retarded in the direction of propagation that is downward for the source fields and upward for the back-scattered fields. Given measurements of the electric and magnetic fields at the Earth's surface it is possible to separate the downgoing and upgoing fields (Berdichevsky and Zhdanov, 1984). The measured surface expression of the upgoing field can then be used to reconstruct information about the field inside the earth and, hence, estimate the geoelectric structure (Zhdanov and Frenkel, 1983a, b; Lee et al., 1987; Zhdanov, 1988; Zhdanov et al., 1988). As in seismic migration, one could extrapolate the signal received back to reflectors or internal currents by using them as a boundary condition for a diffusion equation; this transformation is usually called an analytic continuation. In the presence of measurement noise, however, this is an unstable process. An alternate procedure is to reverse the time flow of the back-scattered signals received at each site and then diffuse these time-reversed signals downward using the ordinary diffusion equation. The diffused time-reversed fields are called migrated fields. Their amplitude will decay downward and will be very different from the original upgoing field whose amplitude increases downward. The usefulness of the migrated field arises because of the following facts:

1) The phase delay associated with diffusing the time-reversed signals corresponds to a downward phase advance in ordinary time. Thus the downward *phase* behavior of the migrated fields is essentially the same as that of

the original upgoing field and the migrated signal summed for sources at all the sites should exhibit the same constructive interference at internal scatterers as the original field.

2) The noise in the migrated field decays downwards because the migrated field satisfies an ordinary diffusion equation. This contrasts with the explosion of error associated with downgoing analytic continuation by using the signal received itself as a boundary condition for a time-reversed diffusion equation. Thus the phase of the upgoing field inside the earth can be estimated more accurately from the migrated field.

There are a number of algorithms developed for migration of ground-penetrating radar (GPR) reflection profile data (Hogan, 1988; Fisher et al., 1989; Fisher et al., 1992). All these algorithms are based on kinematic similarities between radar and seismic wave propagation and can be considered as the direct implementation of seismic migration techniques to radar data. However, at low frequencies or in conductive environments where conduction currents are big enough, seismic type migration based on the wave equation is no longer appropriate for processing of EM data, because EM fields diffuse into the ground.

There are also several publications concerning the possibility of transforming diffusive EM fields to wavefields (Lavrent'ev et al., 1980; Lee et al., 1989). The integral transform relates the diffusive field in time to a unique wavefield in a time-like domain weighted by an exponentially damped kernel. One can interpret these transformed wavefield data using the conventional techniques developed for the wavefields (say, using ray tomography: Lee and Xie, 1993). The main limitation of this approach is that the integral transform is ill-posed, so the explosion of noise could destroy the results of the transformation if one doesn't apply a regularization.

Here, we investigate a different approach to EM imaging. Instead of transforming the diffusive field into a wavefield, we transfer the principles of wavefield analysis to interpretation of the EM fields, which are governed by diffusion equations. Thus we develop the method of EM migration.

First, we review some general ideas concerning seismic migration, or seismoholography. Suppose that we have a local source of seismic waves, located at some point on the earth's surface, and an array of receivers. Each receiver records oscillations at the earth's surface as a function of real time t. We introduce the reverse time

$$\tau = -t. \tag{1}$$

Now replace the receivers by auxiliary sources and make each of these sources operate in reverse time with a signal equal to the recording of the earth's surface oscillating in real time at the corresponding receiver. It is shown in the theory of seismic migration that this field is back propagating, that is, it goes from the observation surface into the earth (Claerbout, 1985). If we recalculate the back propagated, or migrated, field at any interior point of the medium at times corresponding to the arrivals of the direct waves from the actual source, the amplitude distribution of the migrated field will depict the positions of the reflectors and the diffraction points. Thus the restoration of the seismic image of the geological cross-section

is attained by assigning reverse time pseudo-sources to the receiver sites on the earth's surface.

The analogous approach in principle may be applied to the interpretation of EM field data as well. Let us consider the situation where we have measured the total EM field, because of natural sources in the ionosphere or a controlled source. The system of synchronized receivers is located at the surface of the earth. We can replace the receivers by a system of artificial current or charge sources, which are determined by the observed EM field. When these artificial sources operate in reverse time, they produce a field that we will call the *migrated EM field.* As in the seismic case, this field in principle can "delineate" boundaries of the internal structure of the Earth and give us the "geoelectric image" of the earth interior.

MATHEMATICAL CONCEPTS

Now we will give a stricter definition for EM migration. This definition is much more general than one given in our previous publications. However, in the special case of a homogeneous background cross-section it is reduced to the original definition.

Consider a model in which the horizontal plane $z = 0$ separates the conductive Earth ($z > 0$) from a nonconducting atmosphere ($z < 0$). The conductivity of the Earth a(r) is an arbitrary function of the coordinates that can be represented as the sum of normal conductivity σ_n (r) and an anomalous conductivity $\Delta\sigma(r)$ so that a(r) = $\sigma_n(r) + \Delta\sigma(r)$. The EM field in the model is excited by arbitrary sources, located in the ionosphere or at the surface of the Earth. Field components observed on the Earth's surface are denoted by

$$\{E_x^0(r, t), E_y^0(r, t), 0\}$$

and

$$\{H_x^0(r, t), H_y^0(r, t), H_z^0(r, t)\}.$$

We shall call the *migrated field,* $\mathbf{E}^m (r, \tau)\mathbf{H}^m (r, \tau)$, the field meeting the following conditions:

$$\{E_x^m(r, \tau) \, E_y^m(r, \tau), E_z^m(r, \tau)\}_{z=0}$$
$$= \{E_x^0(r, -\tau), E_y^0(r, -\tau), 0\}_{z=0}, \quad (2)$$

$$\{H_x^m(r, \tau) \, H_y^m(r, \tau) \, H_z^m(r, \tau)\}_{z=0}$$
$$= \{H_x^0(r, -\tau), H_y^0(r, -\tau), -H_z^0(r, -\tau)\}, \quad (3)$$

$$\begin{cases} curl \ \mathbf{H}^m(r, \tau) = \sigma_n(r)\mathbf{E}^m(r, \tau) \\ \\ curl \ \mathbf{E}^m(r, \tau) = -\mu_0 \dfrac{\partial \mathbf{H}^m}{\partial \tau} (r, \tau) \end{cases} \text{for } z \geq 0, \quad (4)$$

$$\{\mathbf{H}^m(r, \tau), \ \mathbf{E}^m(r, \tau)\} \to 0 \text{ for } |r| \to \infty, \ z \geq 0. \quad (5)$$

Thus we see that the migrated field $\mathbf{E}^m$, $\mathbf{H}^m$ is the EM field in the reverse time τ. It is necessary to use the negative of the vertical component of the observed magnetic field at the right side of equation (3) to make the migrated field satisfy Maxwell's equations up to the surface of observation $z = 0$, because the observed field E^0, H^0 satisfies Maxwell's equations in the real time t. In real time $t = -\tau$, the migrated field satisfies the adjoint equations

$$\begin{cases} curl \ \mathbf{H}^m = \sigma_n\mathbf{E}^m \\ \\ curl \ \mathbf{E}^m = \mu_0 \dfrac{\partial \mathbf{H}^m}{\partial t} . \end{cases} \quad (6)$$

These equations imply that the migrated field is propagating in space from receivers to sources. That is to say, it is a back-propagating field.

For the sake of simplicity, consider a situation when the background conductivity of the Earth σ_n is constant. In this case, the electromagnetic field in the model will satisfy the diffusion equation

$$\nabla^2\mathbf{H} - \mu_0\sigma_n \frac{\partial \mathbf{H}}{\partial t} = 0 \ and \ \nabla^2\mathbf{E} - \mu_0\sigma_n \frac{\partial \mathbf{E}}{\partial t} = 0,$$
$$(7)$$

everywhere outside the zones with anomalous conductivity, and we can discuss the problem of migration of any scalar component $P(r, t)$ of the observed EM field. Note first of all that everywhere outside the zones with anomalous conductivity this component would satisfy the equation

$$\nabla^2 P(r, t) - \mu_0\sigma \frac{\partial P(r, t)}{\partial t} = 0. \quad (8)$$

Let $P^0 (r, t)$ stand for any of the components H_x^0, H_y^0, H_z^0, E_x^0, or E_y^0 measured at the Earth's surface. Then we shall call the *migrated field P^m* of the specified scalar component P^0 of the EM field, the field satisfying the conditions

$$P^m(r, \tau)|_{z=0} = P^0(r, -\tau)_{z=0}, \quad (9)$$

and

$$\nabla^2 P^m(r, \tau) - \mu_0\sigma \frac{\partial P^m(r, \tau)}{\partial \tau} = 0 \text{ for } z > 0, \quad (10)$$

$$P^m(r, \tau) \to 0, \quad \text{for } |r| \to \infty, \quad z > 0. \quad (11)$$

Notice that if we substitute the ordinary time t into equation (10) we shall have the adjoint diffusion equation,

$$\nabla^2 P^m(r, -t) + \mu_0\sigma \frac{\partial P^m(r, -t)}{\partial t} = 0. \quad (12)$$

If the ordinary diffusion equation describes the process of field propagation from the sources to the receivers, then equation (12) describes the inverse process of field propagation from the receivers focusing to sources.

Thus, the problem of establishing the migrated field reduces to a continuation of the field P^0 from the Earth's surface to the lower half-space in the reverse time τ. We call the solution of this problem EM migration.

As is seen from the exposition above, the calculation of the migrated field is reduced to a boundary value problem described by the formulas (2)-(5) in general or by the formulas (9)-(11) in the special case of uniform background. Now we can develop different techniques for solving these problems. In the following sections, we briefly describe solution techniques based on spectral representations of the field in the wavenumber-frequency domain and finite-difference approximations.

ANALYTIC CONTINUATION AND MIGRATION IN THE (K, ω)-DOMAIN FOR A MODEL WITH CONSTANT BACKGROUND CONDUCTIVITY

A specified component of the EM field P in the form of the Fourier integral with respect to spatial and time frequencies k_x, k_y, ω is

$$P(r, t) = \frac{1}{8\pi^3} \int \int \int_{-\infty}^{+\infty} P(k_x, k_y, z, \omega)$$

$$\times \exp\left[-i(k_x x + k_y y + \omega t)\right] dk_x \, dk_y \, d\omega, \quad (13)$$

where $P(k_x, k_y, z, \omega)$ is the 3-D Fourier transform of the field component P.

Let us rewrite expression (8) in the frequency domain for the Fourier transform $P(k_x, k_y, z, \omega)$

$$\frac{\partial^2}{\partial z^2} P(k_x, k_y, z, \omega) = v^2 P(k_x, k_y, z, \omega), \quad (14)$$

where $v^2 = (k_x^2 + k_y^2 - i\omega\mu_0\sigma)$, Re $(v) > 0$ is a wavenumber in the (k, ω) domain and $0 < z < d$ with d being the distance from the earth's surface closest to the surface zone with anomalous conductivity. The general solution of the last equation has the form

$$P(k_x, k_y, z, \omega) = P^u(k_x, k_y, \omega)$$

$$\times \exp(vz) + P^d(k_x, k_y, \omega) \exp(-vz), \quad (15)$$

where $P^u(k_x, k_y, \omega)$ and $P^d(k_x, k_y, \omega)$ are the spectrums of the upgoing and downgoing components of the field on the surface of the earth.

Equation (15) solves the problem of EM field downward analytic continuation in the homogeneous layer $0 < z < d$, if we know the upgoing and downgoing parts of the field. We can use the approach developed in Berdichevsky and Zhdanov (1984) for the field separation into the upgoing and downgoing parts. As an illustration, we present the simple technique for field separation in the 2-D case in Appendix A.

Thus the analytic continuation of the downgoing and upgoing (or scattered) parts of the field is described by the formula

$$P^{cd}(k_x, k_y, z, \omega) = P^d(k_x, k_y, 0, \omega) \exp(-vz), \quad (16)$$

$$P^{cu}(k_x, k_y, z, \omega) = P^u(k_x, k_y, 0, \omega) \exp(vz), \quad (17)$$

where P^{cd} and P^{cu} are results of analytic continuation. Because the exponential in equation (17) is growing with depth, the downward continuation of the upgoing field is an unstable, ill-posed procedure, while the downward continuation of the downgoing field is stable.

From the other side, the Fourier transform of the migrated upgoing field $P^{mu}(k_x, k_y, z, \omega)$, according to equation (12) satisfies the equation

$$\frac{\partial^2}{\partial z^2} P^{mu*}(k_x, k_y, z, \omega) = \tilde{v}^2 P^{mu*}(k_x, k_y, z, \omega), \quad (18)$$

where $\tilde{v}^2 = (k_x^2 + k_y^2 + i\omega\,\mu_0\,a>$, asterisk * denotes complex conjugate values, and $0 < z < +\infty$.

Solving the last equation and taking into account condition (11) we arrive at the expression for the complex conjugate spectrum of the migrated upgoing field at a depth z

$$P^{mu*}(k_x, k_y, z, \omega) = P^u(k_x, k_y, 0, \omega) \exp(-\tilde{v}z), \quad (19)$$

where we choose the branch where Re $\tilde{v} = (k_x^2 + k_y^2 + i\omega\mu_0\sigma)^{1/2} > 0$.

Equation (19) gives us the frequency-domain algorithm for migration of the EM field components, which is an EM analog to the migration technique discussed in Gazdag (1978).

Obviously, the function $f(\tilde{v}, z) = \exp(-\tilde{v}z)$ can be regarded as the frequency response of a low-pass, space-time filter. Therefore, the migration transformation of the EM field is a stable procedure.

FINITE-DIFFERENCE MIGRATION IN A 2-D MODEL WITH THE SLOW HORIZONTAL VARIATION OF THE CONDUCTIVITY

For the 1-D geoelectrical model, formulas (16), (17) and (19) will be reduced to the following:

$$P^{cd}(z, \omega) = P^d(0, \omega) \exp(ik_n(z)z), \quad (20)$$

$$P^{cu}(z, \omega) = P^u(0, \omega) \exp(-ik_n(z)z), \quad (21)$$

$$P^{mu*}(z, \omega) = P^u(0, \omega) \exp(-k_n(z)z), \quad (22)$$

where $k^n(z) = \sqrt{i\omega\mu_0\sigma_n(z)}$ is the wavenumber, Re $k_n > 0$; P^{cd}, P^{CU} are results of the analytic continuation of the downgoing and upgoing parts of the field, and P^{mu} is the migrated upgoing field.

Let us now consider the 2-D geoelectrical model and analyze the TE mode first. Following Lee et al. (1987) by the analogy with equations (15), (20), and (21) we can represent the y component of electric field approximately by the formula:

$$E_y(x, z, \omega) = Q_E^d(x, z, \omega)e^{ik_n z} + Q_E^u(x, z, \omega)e^{-ik_n z}, \quad (23)$$

where the coefficients $Q_E^{d,u}$ depend slowly (i.e., continuous within each layer) on depth, and $k_n(x, z, \omega) = \sqrt{i\omega\mu_0\sigma_n(x, z)}$ is a wavenumber and $\sigma_n(x, z)$ is a background conductivity.

Here the term associated with the downward-decreasing exponential function corresponds to the downgoing part of the electric field, and the term associated with the downward increasing exponential function corresponds to the upgoing part of the electric field

$$E_y^d(x, z, \omega) = Q_E^d(x, z, \omega)e^{ik_n z}, E_y^u(x, z, \omega)$$

$$= Q_E^u(x, z, \omega)e^{-ik_n z}. \quad (24)$$

The electric fields $E_y^{d,u}(x, z, \omega)$ everywhere in the lower half-space satisfy the Helmholtz equations

$$\left[\frac{\partial^2}{\partial x^2} + \frac{\partial^2}{\partial z^2}\right] E_y^{d,u}(x, z, \omega) + k_n^2(x, z, \omega) E_y^{d,u}(x, z, \omega) = 0. \quad (25)$$

Magnetic fields can be expressed in terms of the electric fields by the second Maxwell equation

$$H_x^{d,u} = -\frac{1}{i\omega\mu_0} \cdot \frac{\partial E_y^{d,u}}{\partial z}, H_z^{d,u} = \frac{1}{i\omega\mu_0} \frac{\partial E_y^{d,u}}{\partial x}. \quad (26)$$

Substituting the expressions for the electric fields from equation (24) into equation (25), neglecting the derivatives of k_n (i.e., assuming that k_n is locally constant), and omitting the exponential term we have

$$\frac{\partial^2 Q_E^{d,u}}{\partial x^2} + \frac{\partial^2 Q_E^{d,u}}{\partial z^2} \pm 2ik_n \frac{\partial Q_E^{d,u}}{\partial z} = 0, \qquad (27)$$

where "+" stands for downgoing field and "−" stands for upgoing field.

Differentiating the last expressions by z, we have

$$\frac{1}{2ik_n} \frac{\partial^3 Q_E^{d,u}}{\partial x^2 \partial z} + \frac{1}{2ik_n} \frac{\partial^3 Q_E^{d,u}}{\partial z^3} \pm \frac{\partial^2 Q_E^{d,u}}{\partial z^2} = 0. \qquad (28)$$

Adding equations (27) and (28) with the proper sign and neglecting the third derivative of $Q_E^{d,u}$ by z gives

$$\frac{\partial^3 Q_E^{d,u}}{\partial x^2 \partial z} = \mp 2ik_n \frac{\partial^2 Q_E^{d,u}}{\partial x^2} + (2ik_n)^2 \frac{\partial Q_E^{d,u}}{\partial z}, \qquad (29)$$

where "+" stands for downgoing field and "−" stands for upgoing field.

Solving the last equations numerically and substituting the results in equation (24), we find the upgoing and downgoing components of the field inside the Earth. The corresponding numerical method is discussed in Appendix B.

Now let us consider the TM mode. For this model by the analogy with equation (23) we can represent they component of magnetic field approximately by the following formula:

$$H_y(x, z, \omega) = Q_M^d(x, z, \omega)e^{ik_n z} + Q_M^u(x, z, \omega)e^{-ik_n z}, \qquad (30)$$

where $Q_M^{d,u}$ are the magnetic coefficients that slowly depend on depth. Here the term associated with the downgoing exponential function corresponds to the downgoing part of the field and the term associated with the upgoing exponential function corresponds to the upgoing part of the field

$$H_y^d(x, z, \omega) = Q_M^d(x, z, \omega)e^{ik_n z},$$

$$H_y^u(x, z, \omega) = Q_M^u(x, z, \omega)e^{-ik_n z}. \qquad (31)$$

Magnetic fields $H_y^{d,u}(x, z, \omega)$ everywhere in the lower half-space satisfy the equation

$$\left[\frac{\partial}{\partial x} \left(\frac{1}{k_n^2(x, z, \omega)} \frac{\partial}{\partial x} \right) + \frac{\partial}{\partial z} \left(\frac{1}{k_n^2(x, z, \omega)} \frac{\partial}{\partial z} \right) \right]$$
$$\times H_y^{d,u}(x, z, \omega) + H_y^{d,u}(x, z, \omega) = 0. \qquad (32)$$

Electric fields can be expressed in terms of the magnetic fields by the first Maxwell equation

$$E_x^{d,u} = -\frac{1}{\sigma_n} \frac{\partial H_y^{d,u}}{\partial z}, \quad E_z^{d,u} = \frac{1}{\sigma_n} \frac{\partial H_y^{d,u}}{\partial x}. \qquad (33)$$

Substituting the expressions for the magnetic field from equation (31) into equation (32) and repeating the transformations described above, we obtain

$$\frac{\partial^3 Q_M^{d,u}}{\partial x^2 \partial z} = \mp 2ik_n \frac{\partial^2 Q_M^{d,u}}{\partial x^2} + (2ik_n)^2 \frac{\partial Q_M^{d,u}}{\partial z}, \qquad (34)$$

where "+" stands for downgoing field and "−" stands for upgoing field.

In the case of migration taking into account equation (22), we use the following formulas for the downward extrapolation of the upgoing fields

$$E_y^{mu*}(x, z, \omega) = Q_E^m(x, z, \omega)e^{-k_n z}, \qquad (35)$$

$$H_y^{mu*}(x, z, \omega) = Q_M^m(x, z, \omega)e^{-k_n z}. \qquad (36)$$

In this case, the migrated upgoing electric field $E_y^{mu}(x, z, \omega)$ everywhere in the lower half-space satisfies the following Helmholtz type equation:

$$\left[\frac{\partial^2}{\partial x^2} + \frac{\partial^2}{\partial z^2} \right] E_y^{mu*}(x, z, \omega)$$
$$- k_n^2(x, z, \omega)E_y^{mu*}(x, z, \omega) = 0, \qquad (37)$$

while the migrated upgoing magnetic field $H_y^{mu}(x, z, \omega)$ satisfies the equation

$$\left[\frac{\partial}{\partial x} \left(\frac{1}{k_n^2(x, z, \omega)} \frac{\partial}{\partial x} \right) + \frac{\partial}{\partial z} \left(\frac{1}{k_n^2(x, z, \omega)} \frac{\partial}{\partial z} \right) \right]$$
$$\times H_y^{mu*}(x, z, \omega) - H_y^{mu*}(x, z, \omega) = 0. \qquad (38)$$

Combining equations (35), (36) and (37), (38) and repeating the transformations described above we obtain

$$\frac{\partial^3 Q_{E,M}^{mu}}{\partial x^2 \partial z} = 2k_n \frac{\partial^2 Q_{E,M}^{mu}}{\partial x^2} + (2k_n)^2 \frac{\partial Q_{E,M}^{mu}}{\partial z}. \qquad (39)$$

Equations (29), (34), and (39) contain only first-order vertical derivatives of $Q_{E,M}^{d,u,m}$. Therefore, by means of these equations it is possible to extend separately the downgoing and upgoing parts of the total electric or magnetic field known at the level z to the deeper level $z + \Delta z$, using the finite-difference approximation to equations (29), (34) and (39). A detailed description of this algorithm is presented in Appendix B. The important conclusion is that in the framework of the model with the slow conductivity variation, we can use the same numerical code for migration of both the electric field in the TE mode and the magnetic field in the TM mode.

IMAGING GEOELECTRIC BOUNDARIES BY MIGRATION

In this section, we formulate the principles of underground imaging, based on EM migration. Initially, let us consider a two-layered model with the slow variation of conductivity $\sigma_\ell(x, z)$ and $\sigma_{\ell+1}(x, z)$ within each layer and sharp conductivity contrast on the quasi-horizontal boundary S between two layers.

First we analyze the behavior of the horizontal component of the electric field (TE mode) at the quasi-horizontal boundary $\{S: (x, z_S(x))\}$ between two layers. In the first layer, according to equation (24) we have

$$\begin{cases} E_y(x, z, \omega) = Q_E^d(x, z, \omega)e^{ik_\ell z} + Q_E^u(x, z_S, \omega)e^{-ik_\ell z} \\ E_y'(x, z, \omega) = ik_\ell Q_E^d(x, z, \omega)e^{ik_\ell z} - ik_\ell Q_E^u(x, z, \omega)e^{-ik_\ell z}, \end{cases} \qquad (40)$$

where prime denotes the vertical derivative of the electric field
In the second layer we can write

$$\begin{cases} E_y(x, z, \omega) = Q_E(x, z, \omega)e^{ik_{\ell+1} z} \\ E_y'(x, z, \omega) = ik_{\ell+1} Q_E(x, z, \omega)e^{ik_{\ell+1} z}. \end{cases} \qquad (41)$$

On the boundary $S(z = z_s(x))$ in the case of E-polarization both components E_y and E_y' are continuous. Therefore, the corresponding right-hand sides of equations (40) and (41) are equal. Solving this system of equations, we find

$$\frac{Q_E^u}{Q_E^d} = \beta^{(\ell)}(x, z_S)e^{2ik_\ell z_S}, \qquad (42)$$

where

$$\beta^{(\ell)}(x, z_S) = \frac{\sqrt{\sigma_\ell(x, z_S)} - \sqrt{\sigma_{\ell+1}(x, z_S)}}{\sqrt{\sigma_\ell(x, z_S)} + \sqrt{\sigma_{\ell+1}(x, z_S)}} \qquad (43)$$

is the so-called *reflectivity coefficient*.

Let us calculate the electric apparent reflectivity function as the ratio of the upgoing and downgoing electric fields:

$$\beta_{Ea}(x, z, \omega) = \frac{E_y^u(x, z, \omega)}{E_y^d(x, z, \omega)} = \frac{Q_E^u(x, z, \omega)}{Q_E^d(x, z, \omega)}e^{-2ik_\ell z}. \quad (44)$$

According to equation (42), at the boundary S

$$\beta_{Ea}(x, z_S, \omega) = \beta^{(\ell)}(x, z_S). \qquad (45)$$

So, at the geoelectrical boundary, the electric apparent reflectivity function is exactly equal to the true reflectivity coefficient!

In the case of the TM mode we can repeat all these calculations for the horizontal component of the magnetic field H_Y. As the result, we obtain

$$\frac{Q_M^u}{Q_M^d} = -\beta^{(\ell)}(x, z_S)e^{2ik_\ell z_S}. \qquad (46)$$

Therefore we can introduce the magnetic apparent reflectivity function as the ratio of the upgoing and downgoing magnetic fields (note the minus sign)

$$\beta_{Ma}(x, z, \omega) = -\frac{H_y^u(x, z, \omega)}{H_y^d(x, z, \omega)} = -\frac{Q_M^u(x, z, \omega)}{Q_M^d(x, z, \omega)}e^{-2ik_\ell z} \qquad (47)$$

According to equation (46) at the boundary

$$\beta_{Ma}(x, z_S, \omega) = \beta^{(\ell)}(x, z_S). \qquad (48)$$

So, at the geoelectrical boundary magnetic apparent reflectivity function is also equal exactly to the true reflectivity coefficient.

Thus we see that although the phases of the downgoing and upgoing electric and magnetic fields $\varphi_E^{d,u}(x, z, \omega)$ and $\varphi_M^{d,u}(x, z, \omega)$ in general depend on the frequency ω, close to the geoelectric boundaries their difference becomes approximately independent of frequency, according to equations (45) and (48) (because the reflectivity coefficient $\beta^{(\ell)}$ is real). From the physical point of view, we have the effect analogous to the seismic case, when the primary (downgoing) and scattered (upgoing) components of the field have the same phase at the position of a reflector. This property of the wavefield is usually used as an imaging condition in a seismic phase migration algorithm (Claerbout, 1985). We can use this imaging condition for electromagnetic fields as well, in which a geoelectric boundary plays the role of a reflector.

We can express electric or magnetic apparent reflectivity functions $\beta_{E\ Ma}(r, \omega)$ as

$$\beta_{Ea}(x, z, \omega) = E_y^u/E_y^d = |E_y^u/E_y^d| \exp(i(\varphi_E^u - \varphi_E^d)). \quad (49)$$

$$\beta_{Ma}(x, z, \omega) = -H_y^u/H_y^d = |H_y^u/H_y^d| \exp(i(\varphi_M^u - \varphi_M^d \pm \pi)). \qquad (50)$$

The normalized values of $\beta_{E,Ma}$ depend only on the phases differences

$$\beta_{Ea}^n = \frac{\beta_{Ea}}{|\beta_{Ea}|} = \exp(i(\varphi_E^u - \varphi_E^d));$$

$$\beta_{Ma}^n = \frac{\beta_{Ma}}{|\beta_{Ma}|} = \exp(i(\varphi_M^u - \varphi_M^d \pm \pi)). \qquad (510$$

We have mentioned above that if the point of observation (x, z) approaches the geoelectrical boundary S, then

$$\varphi_{E,M}^u(x, z, \omega) - \varphi_{E,M}^d(x, z, \omega) \to \Delta\varphi(x, z), \qquad (52)$$

where $\Delta\varphi(x, z)$ doesn't depend on frequency (it is equal to 0 or π). Therefore we see that the phase of $\beta_{E\ Ma}^n$ is significantly frequency dependent except at an interface of high conductivity gradient, where it will be approximately independent of frequency. Thus, stacking $\beta_{E,Ma}^n$ for a spectrum of frequencies $(\omega_1 < \omega_2 < \omega_3 < \cdots < \omega_J)$ results in positive reinforcement at interfaces and destructive interference elsewhere:

$$\bar\beta_{E,Ma}^n(x, z) = \frac{1}{J}\sum_{j=1}^J \beta_{E,Ma}^n(x, z, \omega_j) \qquad (53)$$

and

$$\bar\beta_{E,Ma}^n(x, z)_{J\to\infty} \to 0, \ if \ (x, z) \notin S;$$
$$\bar\beta_{E,Ma}^n(x, z)_{J\to\infty} \to 1, \ if \ (x, z) \in S. \qquad (54)$$

The same consideration can be applied not only to a two-layered model, but to a multilayered cross-section as well. Indeed, consider the N-layered model with the slow variation of conductivity $\sigma_\ell(x, z)$ within each layer ($\ell = 1, 2, \ldots N$) and sharp conductivity contrast on the quasi-horizontal boundaries S_ℓ between the ℓth and $(\ell + 1)$-th layers. For any given boundary S_ℓ one can select a frequency $\omega^{(\ell)}$ so high that the skin depth $\delta(\omega^{(\ell)})$ of the field penetration inside the Earth is less than the depth to the boundary $S_{\ell+1}$:

$$\delta(\omega^{(\ell)}) < z_{S_{\ell+1}}, if \ \omega > \omega^{(\ell)}. \qquad (55)$$

In this case, one has exactly the same expressions for the field components inside the ℓth and $(\ell + 1)$-th layers as equations (40) and (41). Therefore, we can repeat all the mathematical analysis described above and obtain the same results. The only difference is that now the stacking of the normalized apparent reflectivity functions for different depths (z) corresponding to the skin depth $\delta(\omega_{j_0})$ has to be done for different frequency intervals:

$$\bar\beta_{E,Ma}^n(x, z = \delta(\omega_{j_0})) = \frac{1}{J - j_0 + 1}\sum_{j=j_0}^J \beta_{E,Ma}^n(x, z, \omega_j), \qquad (56)$$

where ω_{j_0} is the lowest frequency of the stacking interval (ω_{j_0}, ω_J). The procedure described above is analogous to the conventional vertical sounding of the geoelectrical cross section: when we migrate the field to shallow depth we use only high frequencies, while migrating deeper we involve more lower frequencies in the calculations, thus "scanning" the vertical cross section.

It is important to emphasize that for this kind of imaging it is necessary to reconstruct only the phase of the upgoing field

inside the conductive earth. If we compare the phase frequency characteristics of the analytical continuation of the upgoing field [equation (17)] and of its complex conjugate migration [equation (19)], we see that they are equal! That means that the complex conjugate migrated upgoing field has the same phases as the upgoing field itself. Therefore for imaging we can use the migrated reflectivity function $\beta_{E,Mm}(x, z, \omega)$, equal to

$$\beta_{Em} = E_y^{um*}/E_y^d, \text{ or } \beta_{Mm} = -H_y^{um*}/H_y^d, \quad (57)$$

where E_y^{um*}, $H_\cdot^{um}*$ are the complex conjugate migrated upgoing fields. The inphase summation of the migrated reflectivity functions indicates the position of the boundaries between layers with different conductivities.

Now we can demonstrate the imaging principles for simple synthetic structures, thus providing evidence of the stability of EM migration. For practical calculations we have developed a simplified migration code, which is based on the assumption of a constant background conductivity. Note that in this paper we discuss mainly the results of numerical modeling for plane-wave excitation. In principle, the same approach is applicable for the controlled-source data as well, however, this problem remains to be analyzed and examined.

Figure 1a depicts a model of a 2-D step-wise structure. Figure 2a and Figure 2b show the corresponding apparent resistivity and phase pseudosections, computed for the TE mode. Migration in the frequency domain is realized by a finite-difference method. The migrated field $E^{um}(x, z)$ corresponding to the surface values of the upgoing part of the observed field $E_y^u(x, 0)$ in the model was calculated in the lower half-space, using a finite-difference algorithm. The migrated reflectivity function $\beta_{Em}(x, z, \omega)$ was then calculated for each position (x, z) and each frequency ω. As we have shown above, stacking β_{Em} for a spectrum of frequencies results in positive reinforcement at interfaces and destructive interference elsewhere. Figure 2c shows a stacked normalized apparent reflectivity function $\bar{\beta}_{Ea}^n(x, z)$. The maximum in $\bar{\beta}_{Ea}^n(x, z)$ shown in Figure 2c almost coincides with the interface between two layers, which clearly demonstrates the phase coherence of the migrated field near the reflector. Thus the migration image produces the correct position of the interface.

Figure 2f shows the same model derived from surface data to which 20% Gaussian noise was added as shown on the apparent resistivity and pseudo-sections in Figure 2d and Figure 2e. Nevertheless one can see that the result of the migration produced a rather clear image of the interface.

Figure 1b depicts a locally conductive rectangular-insert 2-D model. The resistivity of the inclusion is 0.5 ohm•m, and the resistivity of the host rocks is 50 ohm•m. Corresponding apparent resistivity and phase pseudosections are shown in Figure 3a and Figure 3b. The local maximum in $\bar{\beta}_{Ea}^n(x, z)$ almost coincides with the top boundary of the anomalous structure (Figure 3c). Figure 3d and Figure 3e depict the response of the same model, but with 20% Gaussian noise added. The result of migration is shown in Figure 3f. The image becomes a little narrower, but still delineates the top boundary of the inclusion. Figure 1c presents a 2-D model with three conductive rectangular inserts with resistivities 0.5 ohm•m within a 50 ohm•m background. These individual conductive bodies cannot be seen on the pseudosection of apparent resistivity (Figure 4a), and the phase pseudosection (Figure 4b), but they can easily be imaged by migration

(Figure 4c). We have the same result even if we add 20% Gaussian noise to the observed data (Figure 4d, 4e, and 4f).

Thus for these models EM migration produces stable images of the top geoelectrical interfaces.

RESISTIVITY IMAGING

In practical applications, it is very important to be able to plot not only the geometry of the boundaries, but also the resistivity distribution. We discuss here the technique for the solution of this problem, based on the analysis of the vertical distribution of the reflectivity function for the same multilayered model introduced in the previous section. We begin our analysis with the two-layered model. We have shown above
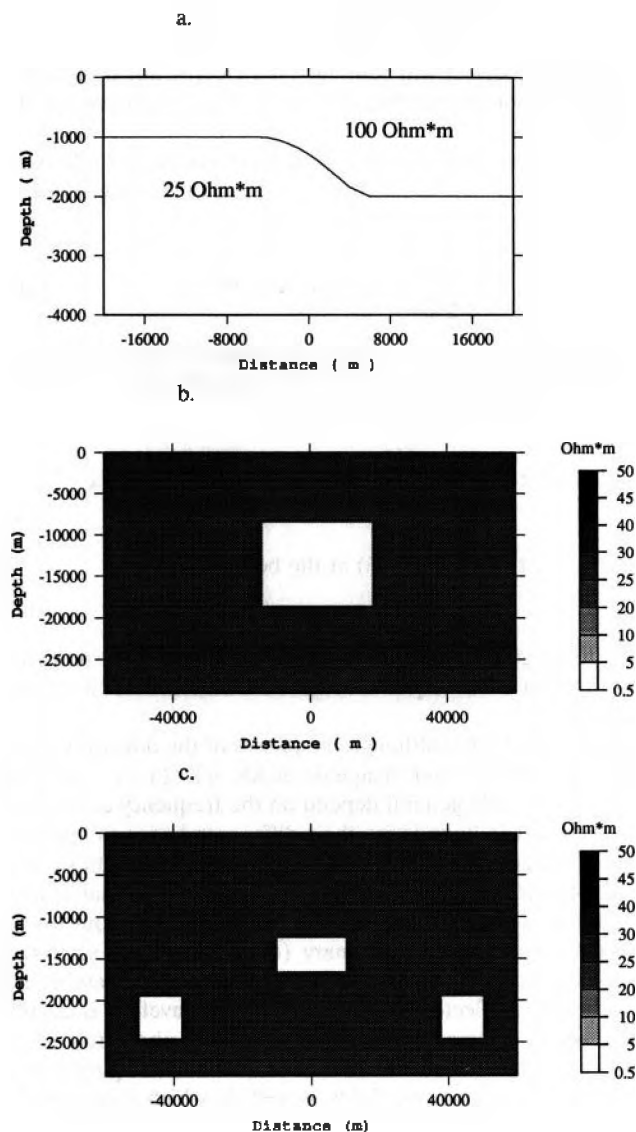

FIG. 1. Three 2-D resistivity models used to illustrate imaging geoelectric boundaries by EM migration. (a) Resistivity model of a step-wise structure. (b) Resistivity model with a locally conductive rectangular insert (resistivity of the inclusion is 0.5 ohm•m, resistivity of the host rock is 50 ohm • m). (c) Resistivity model with three conductive rectangular inserts (resistivity of the inclusions is 0.5 ohm • m, resistivity of the host rock is 50 ohm • m).

that the reflectivity function $\beta_{E,Ma}(x, z, \omega)$ at the depth of a geoelectrical boundary is equal to the true coefficient of reflectivity $\beta_1 = (\sqrt{\sigma_1} - \sqrt{\sigma_2})/(\sqrt{\sigma_1} + \sqrt{\sigma_2})$. Therefore the resistivity of the underlying layer ρ_2 can be calculated as

$$\rho_2 = \left\{ \frac{[1 + \bar{\beta}_{E,Ma}(x, z)]}{[1 - \bar{\beta}_{E,Ma}(x, z)]} \right\}^2 \rho_1, \qquad (58)$$

where

$$a_{E,Ma}(x, z) = \frac{1}{J} \sum_{j=1}^{I} \beta_{E,Ma}(x, z, \omega_j). \qquad (59)$$

On the other side, we know that stacking the migrated reflectivity function $\beta_{E,Mm}(x, z, \omega_j)$ for a spectrum of frequencies results in positive reinforcement at interfaces and destructive interferences elsewhere. We can introduce a normalized stacked migrated reflectivity function $\bar{\beta}_{E,Mm}^n(x, z)$ as

$$\bar{\beta}_{E,Mm}^n(x, z) = \frac{1}{N} \sum_{j=1}^{N} \frac{\beta_{E,Mm}(x, z, \omega_j)}{|\beta_{E,Mm}(x, z, \omega_j)|} \qquad (60)$$

and calculate the migrated apparent resistivity $\rho_m(x, z)$ as
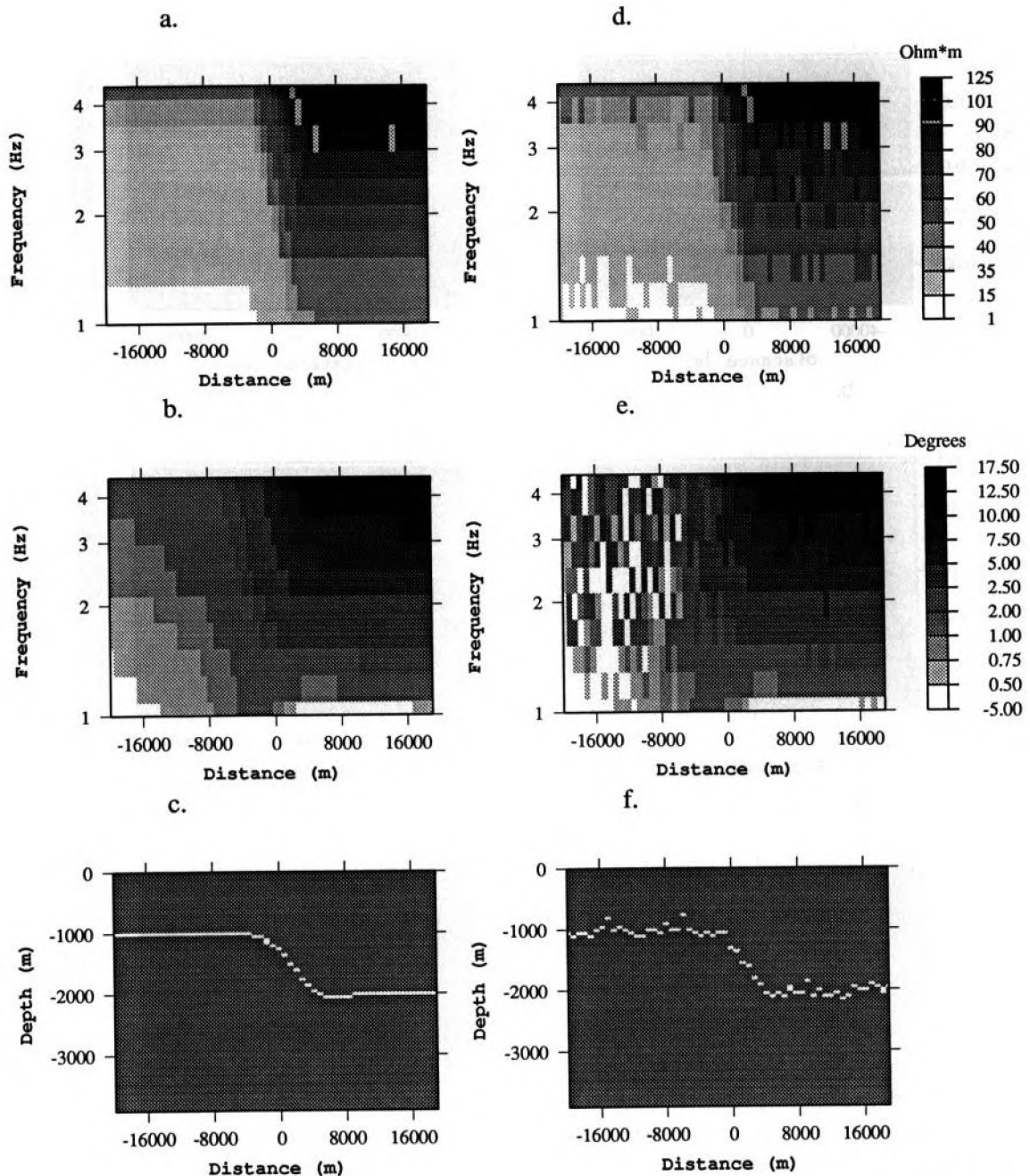

FIG. 2. Apparent resistivity (a) and (d), E_Y phase pseudosections (b) and (e), and migration images (c) and (f) for the step-wise structure [model (a) in Figure 1] without (left panel) and with (right panel) 20% Gaussian noise.

$$\rho_m(x, z) = \left\{ \frac{[1 + \bar{\beta}^n_{E,Mm}(x, z)\bar{\beta}_{E,Ma}(x, z)]}{[1 - \bar{\beta}^n_{E,Mm}(x, z)\bar{\beta}_{E,Ma}(x, z)]} \right\}^2 \rho_1. \quad (61)$$

The migrated apparent resistivity $\rho_m(x, z)$ is equal to the resistivity of the second layer at the interface and is equal to the resistivity of the background ρ_1 elsewhere, because $\beta^n_{E,Mm}(x, z) \rightarrow 1$ at the interfaces and $\beta^n_{E,Mm}(x, z) \rightarrow 0$ elsewhere. Here, we use two reflectivity functions, apparent and migrated, to obtain a stable image of the geoelectric boundary and the resistivity contrast at the boundary simultaneously.

The resistivity of the first layer ρ_1 can be found from the observed electromagnetic fields using the classical formulas. For example, in the case of plane-wave excitation we can use the admittance $Y(w)$ estimated for a high enough frequency:

$$\rho_1 = 1/2\omega\mu_0 Re^2 Y(\omega) = 1/2\omega\mu_0 Im^2 Y(\omega). \quad (62)$$

The algorithm described admits a simple generalization for the case of a multilayered background geoelectrical cross section. Indeed in this case the procedure of visualizing geoelectrical boundaries is realized successfully in a downward
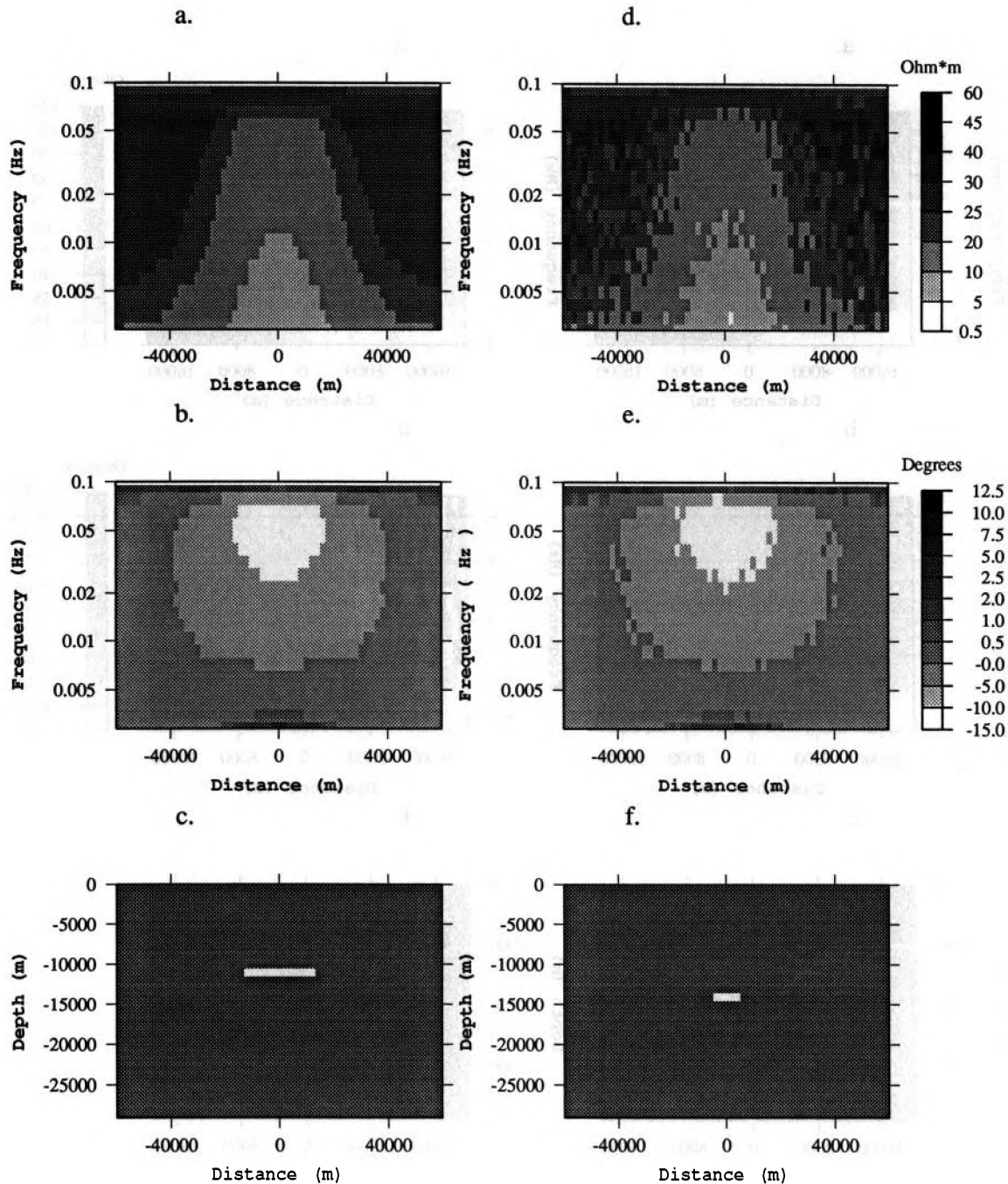
FIG. 3. Apparent resistivity (a) and (d), E_y phase   seudosections (b and (e), and migration images (c) and (f) for the model with a locally conductive rectangular insert [model (b in Figure 1] without (left panel) and with (right panel) 20% Gaussian noise.

direction, and in each stage a band of frequencies is chosen at which the field penetrates the layers studied. In the first stage a specific electric resistivity of the first layer ρ_1 is evaluated by a standard formulas like equation (62). In the second stage, an analytic continuation (or migration) is made into the medium featuring the electric resistivity ρ_1, and the reflectivity function $\beta_{E,Ma}(x, z, \omega)$, and the migrated reflectivity function $\beta_{E,Mm}(x, z, \omega)$ are calculated. From the local maximum of the stacked reflectivity functions, the position of the top of the second layer and its specific electric resistivity ρ_2 are evaluated. Then the migration and analytic continuation procedures are repeated but with a new parameter for the background medium ρ_2. From the space-frequency distribution of the conventional and migrated reflectivity functions we find the top of the third layer and its resistivity, and so on.

We can also generalize equation (61) for the model with the inhomogeneous (but slowly horizontally varying) background resistivity $\rho_n(x, z)$:
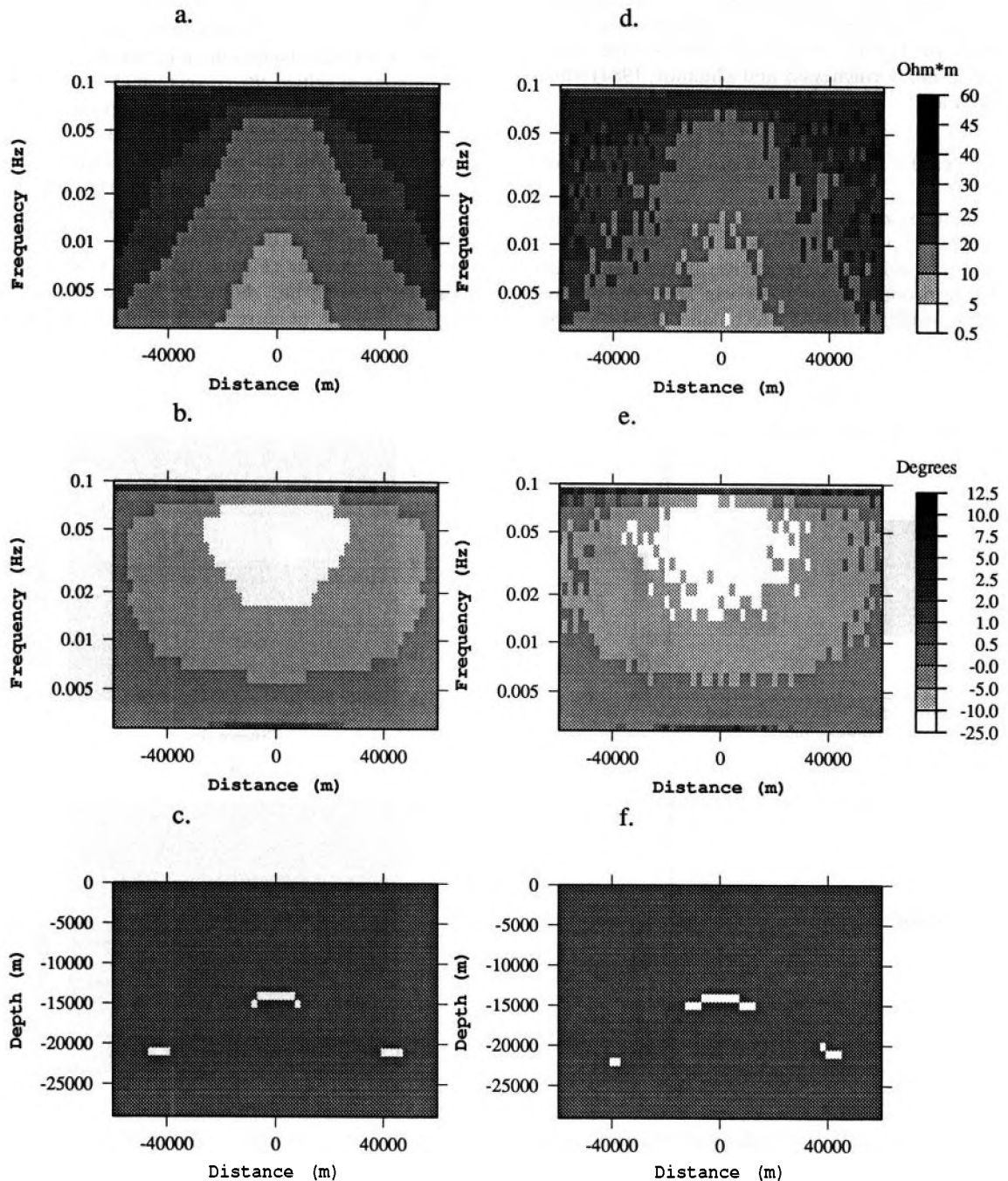

FIG. 4. Apparent resistivity (a) and (d), E_y phase pseudosections (b) and (e), and migration images (c) and (f) for the model with three conductive rectangular inserts [model (c) in Figure 1] without (left panel) and with (right panel) 20% Gaussian noise.

$$\rho_m(x,z) = \left\{ \frac{[1 + \bar{\beta}^n_{E,Mm}(x,z)\bar{\beta}_{E,Ma}(x,z)]}{[1 - \bar{\beta}^n_{E,Mm}(x,z)\bar{\beta}_{E,Ma}(x,z)]} \right\}^2 \rho_n(x,z). \quad (63)$$

Here, stacking of the reflectivity functions is done according to expression (56) at the stacking interval (ω_{j_0}, ω_J) where ω_{j_0} is the frequency corresponding to the skin depth $z = \delta(\omega_{j_0})$.

The last formula produces the resistivity of the underlying layer in the location of the interfaces and is equal to the background resistivity elsewhere.

The main difficulty in realizing this approach is determining the background resistivity distribution $\rho_n(x, z)$. This problem can be solved, at least approximately, by various algebraic or differential transformations of the apparent resistivity curve. The most suitable transformation seems to be Niblett or Bostick transform (Niblett and Sayn-Wittgenstein, 1960; Berdichevsky and Zhdanov, 1984) which can be written as:

$$\rho_n(x, z) = 1 \left/ \frac{d}{dz}\left(\frac{z}{\rho_a}\right) \right. = \rho_a \frac{2 + m}{2 - m}, \quad (64)$$

where $m = d \log \rho_a / d \log \sqrt{T}$, $T = 2\pi/\omega$ and z is defined as effective depth of penetration: $z = \sqrt{T\rho_a/2\pi\mu_0}$.

To obtain the background resistivity distribution model with the slow horizontal variation, we can apply the electromagnetic array profiling (EMAP) technique (Bostick, 1986,

Torres-Verdin and Bostick, 1992) and apply some spatial filtering to the observed data. After that we calculate the conventional apparent resistivity and then recalculate it into the background resistivity using the Niblett transform (64). This is the first stage of our rapid imaging technique. In the second stage, we apply a migration transform and determine the migration apparent resistivity using formula (63).

We will illustrate resistivity imaging for a model, containing one resistive and one conductive prismatic inclusions in a homogeneous background (Figure 5a) and in two layered background media (Figure 5b). The models are excited by a vertically propagating plane wave. The bottom parts of Figure 5 present the results of the resistivity imaging by migration (the plots of migrated apparent resistivity ρ_m (x, z)). We can clearly see on these images the top boundaries of the geoelectrical inhomogeneities, the correct values of the resistivities of the background and the inhomogeneities and the position of the top of the second layer on Figure 5d.

We now examine the response of frequency-domain EM migration to host resistivity ρ_h errors. To make this analysis more clear, we consider again the simple model with one conductive body in the host medium with the resistivity $\rho_h = 250$ ohm • m (Figure 6a). The results of migration resistivity imaging are shown in Figure 6b. The migration image, calculated for correct background resistivity $\rho_n = 250$
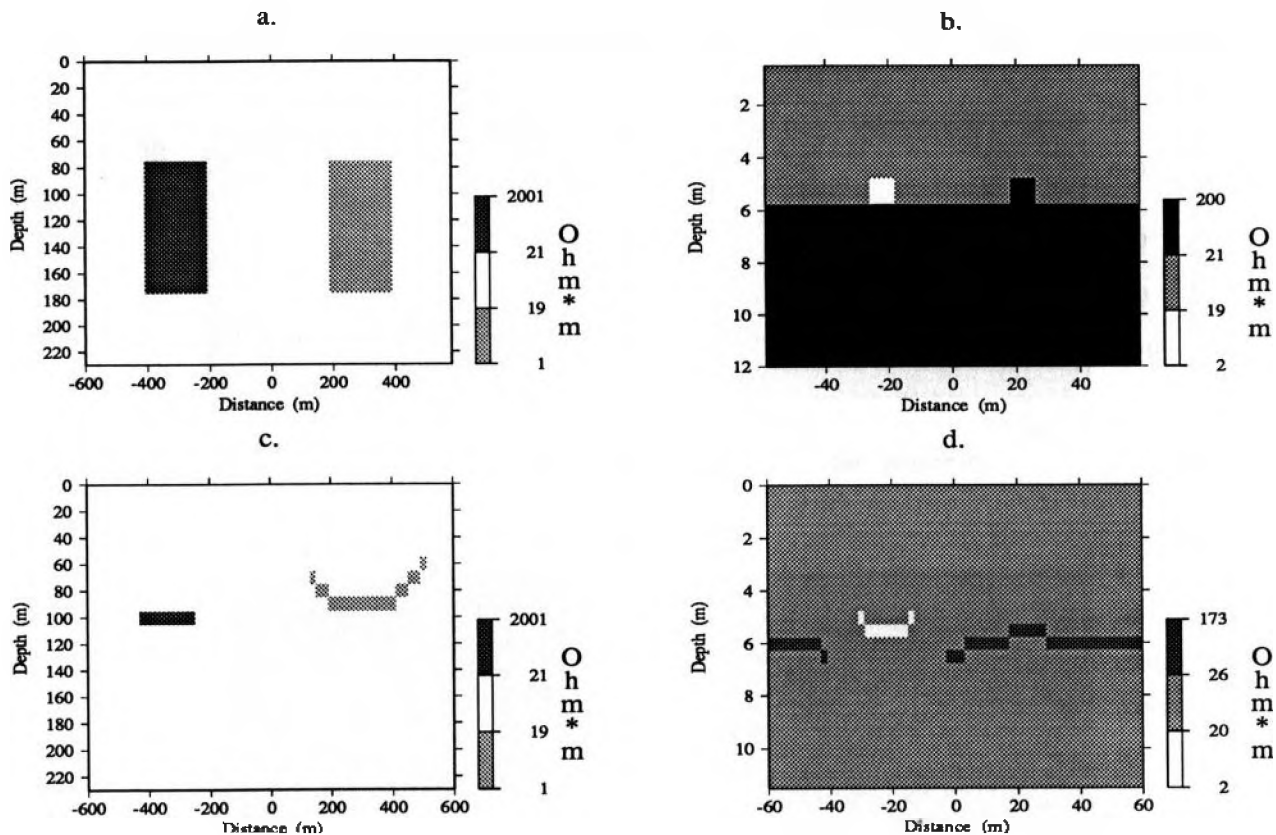

FIG. 5. 2-D resistivity models used to illustrate resistivity imaging by EM migration. (a) Resistivity model with one resistive ($\rho_{i1} = 2000$ ohm • m) and one conductive ($\rho_{i2} = 1$ ohm • m) rectangular inserts in the host medium with the resistivity $\rho_h = 20$ ohm • m. (b) One resistive ($\rho_{i1} = 200$ ohm • m) and one conductive ($\rho_{i2} = 2$ ohm • m) rectangular inserts in the two layered host medium (resistivity of the first layer is $\rho_{h1} = 20$ ohm • m and of second layer is $\rho_{h2} = 200$ ohm • m). (c) Migration resistivity image for model (a). (d) Migration resistivity image for model (b).
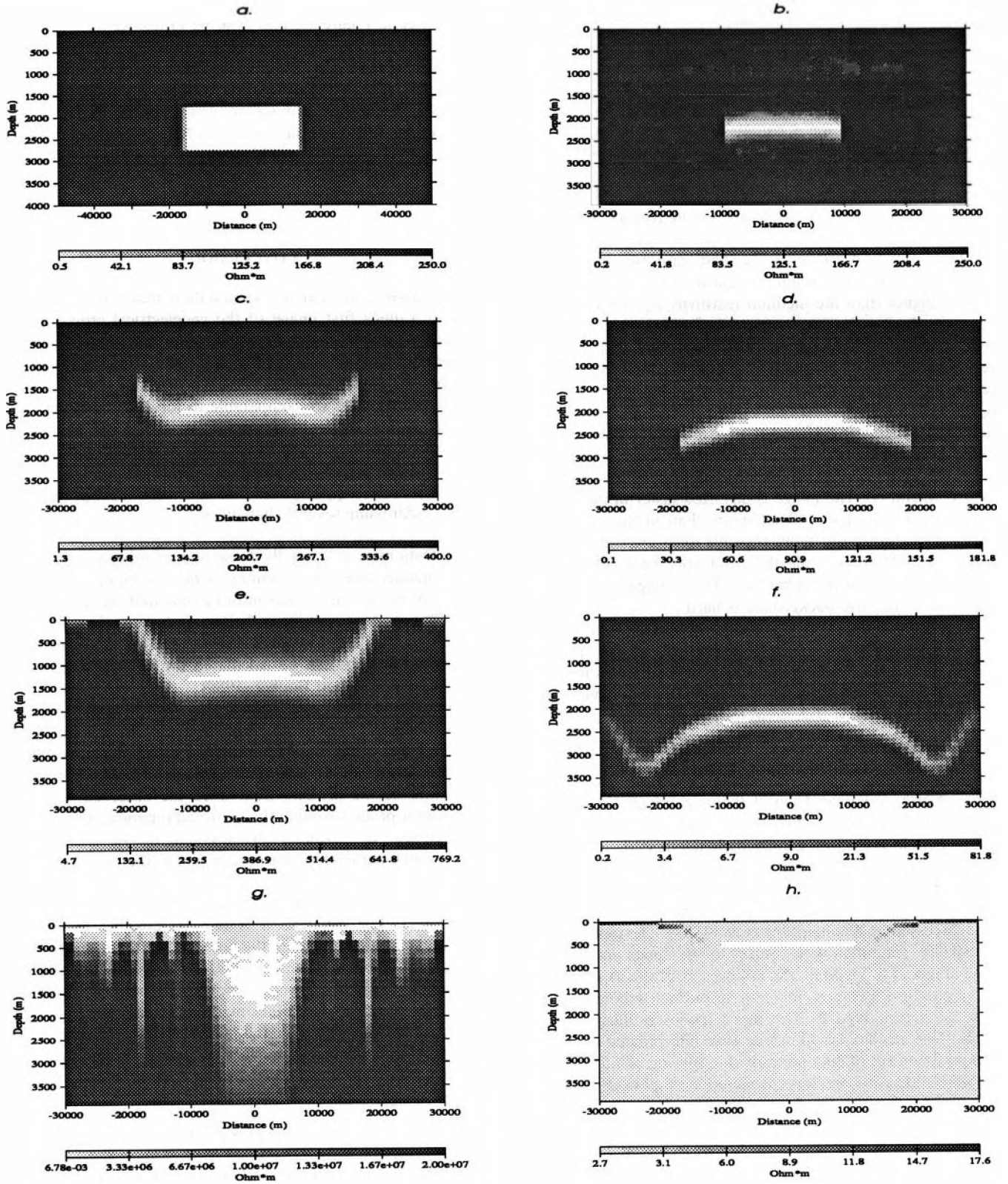
FIG. 6. Study of the response of frequency domain EM migration to host resistivity ρ_n errors. (a) Resistivity model with a locally conductive rectangular insert (resistivity of the insert $\rho_i = 0.5$ ohm • m, host resistivity $\rho_h = 250$ ohm • m). (b) Migration resistivity image, calculated for the correct background resistivity $\rho_n = 250$ ohm • m. (c) Background resistivity ρ_n 60% higher (400 ohm • m) than the actual medium resistivity ρ_h causes "overmigration." (d) Background resistivity ρ_n 30% lower (180 ohm • m) than the actual medium resistivity ρ causes "undermigration." (e), (f) Distortion of the migration resistivity image is stronger when, ρ_n is three times higher than ρ_h [750 ohm • m (e)] or is three times lower than ρ_h [85 ohm • m, (f)]. (g), (h) Migration resistivity image is completely destroyed when ρ_n is more than 10 times higher than ρ_h (g) or is 10 times lower than ρ_h (h).

ohm • m, clearly outlines the top boundary of the body and gives correct estimate of it's resistivity.

Now we increase the background resistivity (ρ_n) to 400 ohm • m. The effect on the migration image is very clear-the left-hand and right-hand edges of the conductive structure go up (Figure 6c), while the central part of the image still describes well the location and the resistivity of the conductive body. If we decrease the background resistivity to $\rho_n = 180$ ohm • m the left-hand and right-hand edges of the conductive structure go down ((Figure 6d), but still the position of the central part of the image is quite correct. This result is very similar to one that takes place in seismic migration (Yilmaz, 1987). Actually in the first case we observe the "overmigration" effect when the resistivity of the background is 60% higher than the medium resistivity ρ_h. In the second case, we observe the "undermigration" effect when the resistivity of the background is 30% lower than the medium resistivity ρ_h. As we amplify the errors in the background resistivity ρ_n (as it is shown in Figure 6e and 6f, where we used ρ_n of 750 ohm l m and 85 ohm•m correspondingly) the distortion level is increasing. However, only if we intensify the errors in the host resistivity determination significantly (to ten times or more), is the image significantly distorted, as it is shown in Figure 6g and 6h. The image is distorted faster in the case of decreasing the background resistivity than in the case of its increasing, because the highly resistive rocks are still transparent to the EM field, while the conductive rocks absorb the EM field because of the skin effect. Thus, imaging of resistive targets in conductive background is hard.

We can conclude that a correct estimation of the background resistivity for migration is important, but the errors in ρ_n do not destroy the image dramatically as long as they are within reasonable limits (no more than one order of magnitude of the host resistivity: $0.2 < |\rho_n/\rho_h| < 5$).

IMAGING THE NORTH AMERICAN CENTRAL PLAINS CONDUCTMTY ANOMALY

The North American Central Plains conductivity anomaly (known as NACP) was first discovered in the late 1960s (Reitzel et al., 1970) by a geomagnetic depth sounding (GDS) array. Jones and Craven (1989) conducted extensive studies of NACP using GDS, seismic and gravity data. We have calculated the forward response of NACP using the finite-element code discussed in Wannamaker et al. (1987). The input model was slightly simplified with respect to the Jones and Craven original model to facilitate the assessment of the capability of the migration scheme to image a subsurface inhomogeneity such as that of NACP. The input model is illustrated in Figure 7a. Calculated field values were interpolated to create an equidistant set of data points with a spacing of 1.5 km. The E-polarization response was calculated at 68 periods over the four decades $0.1\text{-}10^4$ s and was interpolated for contouring.

The resulting image of the migrated field is illustrated in Figure 7b. It is clear that separate bodies in the model are not resolved, but the general geometry of the model and its resistivity are imaged with good quality. Note, that this result corresponds very well to the result of the inversion of the synthetic NACP structures, obtained by the rapid relaxation inversion (RRI) method for TE data (Nong et al., 1993).

We also studied the TM data for the same model. The TM field response was calculated at 68 periods over the four decades $0.1\text{-}10^4$ s as well. The migration image for TM data is presented in Figure 7c. It is possible to resolve all conductive bodies on the TM migration image, although the conductivity is underestimated by TM mode migration. Note, that in this example we use the simplified model of NACP structure without the surface conductor, which makes it possible to resolve the TM mode data. The real NACP response does not show an anomaly in the TM mode. One can expect that the joint TE and TM mode migration will produce the more accurate image, like in the case of RRI inversion (Nong et al., 1993).

CONCLUSIONS

Migration and analytic continuation make it possible to obtain a quick first image of the geoelectrical cross-section, provided one has available continuous profile electromagnetic observations on the surface of the earth, which are phase-referenced. It is important to notice that the computational efforts in this case are comparable to forward modeling. The results of imaging could be used either as the semiqualitative estimation of the geoelectrical model, or as a starting model for more comprehensive inversion algorithms.

The practical application of electromagnetic migration requires addressing several challenges:

1) Data must be spatially dense and must be collected in a manner that preserves intersite phase relations. This does not mean that all sites must be operated simultaneously, but it does require sufficient spatial overlap between separate deployments of instruments that intersite transfer functions can be calculated for all measured fields (see Egbert and Booker, 1989).

2) One must be able to separate the downgoing and upgoing (scattered) fields. In principle, this is accomplished for MT array data (Berdichevsky and Zhdanov, 1984; Zhdanov, 1988). For controlled sources, direct subtraction of the primary field from the observed signal is appropriate to obtain the scattered (upgoing) field, but is subject to errors in measurement of the signals and source parameters, and prediction of the primary field.

Despite these difficulties, EM migration clearly has potential advantages. For instance, it should be possible to quickly generate migrated images in the field and use them to optimize instrument deployments. In addition, migrated images for complicated source-receiver geometries and complex structure should be possible when other methods are not computationally feasible. Also, the migrated image can be used as the first approximation of the subsurface structure in an inversion scheme, based on more sophisticated forward modeling and inversion algorithms.
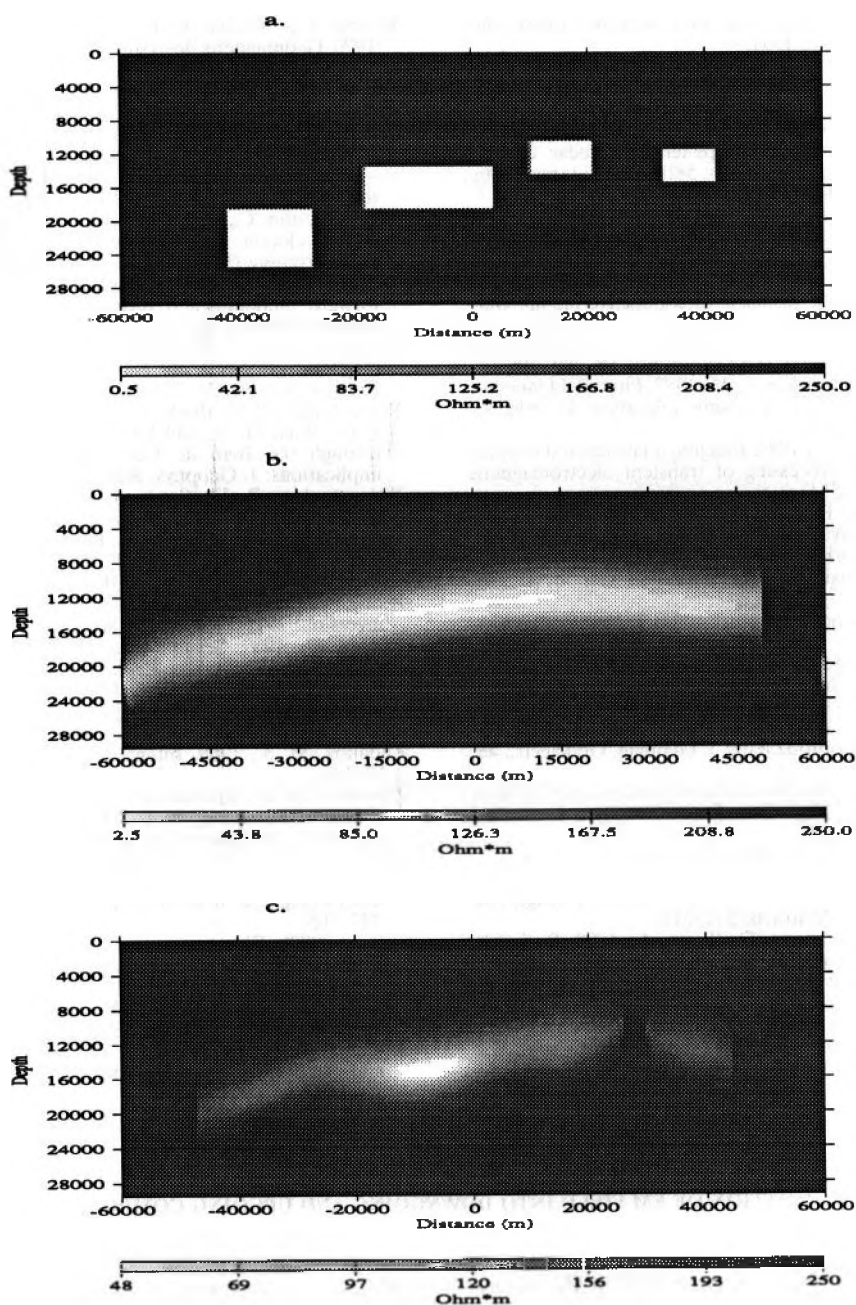
ACKNOWLEDGMENTS

FIG. 7. The North American Central Plains conductivity anomaly. (a) A simplified 2-D resistivity model of the NACP anomaly. (b) Migration resistivity image (TE mode). (c) Migration resistivity image (TM mode).

for forward modeling and for fruitful discussions and comments. We are grateful to A. Tripp for correcting the manuscript and to 0. Portniaguine for help with the visualization code. We particularly thank the reviewers for their helpful and constructive review of this paper.

REFERENCES

Barnett, C. T., 1984, Simple inversion of time-domain electromagnetic data: Geophysics, **49** 925-933.
Berdichevsky, M. N., and Zhdanov, M. S., 1984, Advanced theory of dee geomagnetic sounding: Elsevier Science Publ.
Bosttc, F. X., Jr., 1986, Electromagnetic array profiling: 56th Ann. Internat. Mtg., Soc. Expl. Geophys., Expanded Abstracts, 60-61.
Claerbout, J. F., 1985, Imaging the Earth Interior: Blackwell Sci. Publ.

deGroot-Hedlin, C., and Constable, S. C., 1990, Occam's inversion to generate smooth two-dimensional models from magnetotelluric data: Geophysics, **55,** 1613-1624.
Eaton, P. A., 1989, 3D Electromagnetic inversion using integral equations: Geophys. Prosp., **37,** 407-426.
Eaton, P. A., and Hohmann, G. W., 1989, A rapid inversion technique for transient electromagnetic soundings: PEPI, **53,** 384-404.
Egbert, G. D., and Booker, J. R., 1989, Multivariate analysis of geomagnetic array data I: The response space: J. Geophys. Res., **94,** 14 227-14 248.
Fisher, E., McMechan, G. A., Annan, A. P., and Cosway, S. W., 1992, Examples of reverse-time migration of single-channel, ground-penetrating radar profiles: Geophysics, **57,577-586.**
Fisher, E., McMechan, G. A., Gorman, M. R., Cooper, A. P. R., Aiken, C. L. V., Ander, M. E., and Zumberge, M. A., 1989, Determination of bedrock topography beneath the Greenland ice sheet by three-dimensional imaging of radar sounding data: J. Geophys. Res., **94,2874-2882.**

Gazdag, J., 1978, Wave equation migration with the phase shift method: Geophysics, 43, 1342-135 1.

Jones, A. G., and Craven, J. A., 1990, The North American central plains conductivity anomaly and its correlation with gravity, magnetic, seismic, and heat flow data in Saskatchewan, Canada: Phys. Earth Planet. Inter., 60, 169-194.

Hogan, G., 1988, Migration of ground-penetrating radar data: A technique for locating subsurface targets: 58th Ann. Internat. Mtg., Soc. Expl. Geophys., Expanded Abstracts, 345-347.

Lavrent'ev, M. M., Romanov, V. G., and Shishatsky, S. P., 1980, Ill-posed problems of mathematical physics and analysis: Nauka (in Russian).

Lee, K. H., Liu, G., and Morrison, H. F., 1989, A new approach to modeling the electromagnetic response of conductive media: Geophysics, 54, 1180-1 192.

Lee, K. H., and Xie, G., 1993, A new approach to imaging with low-frequency electromagnetic fields: Geophysics, 58, 780-796.

Lee, S., McMechan, G. A., and Aiken, L. V., 1987, Phasefield imaging: The electromagnetic equivalent of seismic migration: Geophysics, 52, 679-693.

Macnae, J., and Lamontagne, Y., 1987, Imaging quasi-layered conductive structures by simple processing of transient electromagnetic data: Geophysics, 52, 545-554.

Madden, T. R., and Mackie, R. L., 1989, Three-dimensional magnetotelluric modelling and inversion: Proc. IEEE, 77, 2, 318 -332.

Nabighian, M. N., 1979, Quasi-static transient response of a conducting half-space-An approximate representation: Geophysics, 44, 1700-1705.

Nekut, A., 1994, Electromagnetic ray-trace tomography: Geophysics, 59, 371-377.

Niblett, E. R., and Sayn-Wittgenstein, C., 1960, Variation of electrical conductivity with depth by the magnetotelluric method: Geophysics, 25, 948-1008.

Nong, Wr., Booker, J. R., and Smith, J. T., 1993, Rapid two-dimensional inversion of Coprod2 data: J. Geomag. Geoelectr., 45, 1073-1087.

Oldenburg, D., and Li, Y., 1993, Inversion of induced polarization data: 63rd Ann. Internat. Mtg., Soc. Expl. Geophys., Expanded Abstracts, 396-399.

Oldenburg, D. W., Li, Y., and Eliis, R., 1994, Joint interpretation of DC, IP, magnetic, airborne EM, geological, and mineralization data: A case history from Mt. Milligan, 64th Ann. Internat. Mtg., Soc. Expl. Geophys., Expanded Abstracts, 512-515.

Oristaglio, M., Wang, T., Hohmann, G., Tripp, A., 1993, Resistivity imaging of transient electromagnetic data by conjugate-gradient method: 63rd Ann. Internat. Mtg., Soc. Expl. Geophys., Expanded Abstracts, 347-350.

Pellerin, L., Johnston, J., Hohmann G., 1993, Three-dimensional inversion of electromagnetic data: 63rd Ann. Internat. Mtg., Soc. Expl. Geophys., Expanded Abstracts, 360-363.

Reitzel, J. S., Gough, D. I., Porath, D. I., and Anderson, III, C. W., 1970, Geomagnetic deep sounding and upper mantle structure in the western United States: Geophys. J. Roy. Astr. Soc., 19, 213-235.

Samarsky, A. C., 1984, Theory of differencing schemes: Nauka (in Russian).

Smith, J. T., and Booker J. R., 1988, Magnetotelluric inversion for minimum structure: Geophysics, 53, 1565-1576.

——— 1991, Rapid inversion of two- and three-dimensional magnetotelluric data: J. Geophys. Res., 96, 3905-3922.

Torres-Verdin, C., and Bostick, F. X., Jr., 1992, Principles of spatial surface electric field filtering in magnetotellurics: Electromagnetic array profiling (EMAP): Geophysics, 57, 603- 622.

Torres-Verdin, C., and Habashy, T., 1994, Rapid 2.5-dimensional forward modeling and inversion via a new nonlinear scattering approximation: Radio Science, 29, 105 1-1079.

Tripp, A. C., and Hohmann, G. W., 1993, Three-dimensional electromagnetic crosswell inversion: IEEE Trans. on Geoscience and Remote Sensing, 31, 121-126.

Wannamaker, P. E., Booker, J. R., Jones, A. G., Chave, A. D., Filloux, J. H., Waff, H. S., and Law, L. K., 1989, Resistivity cross-section through the Juan de Fuca subduction system and its tectonic implications: J. Geophys. Res., 94, 14 127-14 145.

Wannamaker, P. E., Stodt, J. A., and Rijo, L., 1987, A stable finite-element solution for two-dimensional magnetotelluric modeling: Geop. J. Roy. Astr. Soc., 88, 277-296.

Wessel, P., and Smith, W. H. F., 1991, Free software helps map and display data: EOS Trans. AGU, 72, 441, 445-446.

Xiong, Z., and Kirsch, A., Three-dimensional earth conductivity inversion: 1992 J. Comput. and Applied Math., 42, 109-121.

Yilmaz, O., 1987, Seismic data processing, Series: Investigation in Geophysics, No. 2: Soc. Expl. Geophys.

Zhang, J., Mackie, R., and Madden, T., 3-D resistivity forward modeling and inversion using conjugate gradients: 64th Ann. Internat. Mtg., Soc. Expl. Geophys., Expanded Abstracts, 377-380.

Zhdanov, M. S., 1988, Integral transforms in geophysics: Springer-Verlag.

Zhdanov, M. S., and Booker, J., 1993, Underground imaging by electromagnetic migration: 63rd Ann. Internat. Mtg., Soc. Expl. Geophys., Expanded Abstracts, 355-357.

Zhdanov, M. S., and Frenkel, M. A., 1983a, The solution of the inverse problems on the basis of the analytical continuation of the transient electromagnetic field in reverse time: J. Geomag. Geoelectr., 35, 747-765.

--- 1983b, Electromagnetic migration: in Hjelt, S. E., Ed., 37-58, The development of the deep geoelectric model of the Baltic Shield, Part 2, Univ of Oulu, Oulu.

Zhdanov, M. S., and Keller, G. V., 1994, The electromagnetic methods in geophysical exploration: Elsevier.

Zhdanov, M. S., Matusevich, V. Yu., and Frenkel, M. A., 1988, Seismic and electromagnetic migration: Nauka (in Russian).

APPENDIX A

SEPARATION OF EM FIELD INTO DOWNGOING AND UPGOING COMPONENTS

Here we present the simple technique for field separation in the 2-D case following the approach developed by Berdichevsky and Zhdanov (1984).

Consider a 2-D model with the constant background distribution of conductivity $\sigma_n = const$. Anomalous conductivity is concentrated in some closed domains or in some layer below the Earth's surface. In the layer with constant conductivity σ_n, the E-polarized electric field can be represented as a sum of downgoing and upgoing fields,

$$e_y(k_x, z, \omega) = e_y^d(k_x, \omega) \exp(-vz) + e_y^u(k_x, \omega) \exp(vz),$$

$$(A-1)$$

where $e_y(k_x, z, \omega)$ is the 2-D Fourier transform of the $E_y(x, z, \omega)$ component, $e_y^d(k_x, \omega)$ and $e_y^u(k_x, \omega)$ are the spectra of the downgoing and upgoing components of the field on the surface of the earth, and $v = \sqrt{(k_x^2 - i\omega\mu_0\sigma_n)}$, Re $(v) > 0$ is a wavenumber in (k, ω) domain. From Maxwell's

equations the 2-D Fourier transform $h_x(k_x, z, \omega)$ of the $H_x(x, z, \omega)$ component is

$$h_x(k_x, z, \omega) = \frac{1}{i\omega\mu_0} \frac{\partial e_y}{\partial z} = -\frac{v}{i\omega\mu_0}$$

$$\times [e_y^u(k_x, \omega) \exp(vz) - e_y^d(k_x, \omega) \exp(-vz)]. \quad (A-2)$$

While equations (A-1) and (A-2) give

$$e_y^d(k_x, \omega) = \frac{1}{2}\left[e_y(k_x, 0, \omega) + \frac{i\omega\mu_0}{v} h_x(k_x, 0, \omega)\right]$$

$$e_y^u(k_x, \omega) = \frac{1}{2}\left[e_y(k_x, 0, \omega) - \frac{i\omega\mu_0}{v} h_x(k_x, 0, \omega)\right].$$

$$(A-3)$$

Thus, applying an inverse Fourier transform to both sides of the equations (A-3) gives the downgoing and upgoing components of the electric field on the surface of the earth.